Quiet and perturbed ionospheric representation according to the electron content from GPS signals

Claudio Brunini,[1] María Andrea Van Zele,[2] Amalia Meza,[3] and Mauricio Gende[3]

Received 22 February 2002; revised 14 June 2002; accepted 30 September 2002; published 4 February 2003.

[1] Signals from Global Positioning System (GPS) satellites received at the surface of the Earth have passed through the terrestrial atmosphere and are therefore affected by refraction in the ionosphere. A large number of permanent dual frequencies GPS tracking stations have been built up in the last years and their data have proved to be suitable to study the ionosphere. The main goal of this paper is to assess the capability of these observations to continuously and routinely monitor the ionosphere at a global scale. The interest was focused on retrieving the coefficients of a spherical harmonics expansion that describe the global distribution of the vertical total electron content (VTEC) from the GPS signal. To test our results, we compare them with other GPS-derived results, with VTEC values computed with the International Reference Ionosphere (IRI-95) model, and with direct VTEC determinations provided by Topex-Poseidon satellite. A large set of global VTEC maps with a time resolution of 2 hours was used to describe the evolution of this ionospheric variable at quiet geomagnetic periods during the year 1997. The outstanding features of the VTEC during the 15 May 1997 geomagnetic storm have also been studied. The results show that our method is able to identify large-scale features and seasonal variations of the VTEC in quiet conditions, as well as its variations during a large geomagnetic storm. *INDEX TERMS:* 2447 Ionosphere: Modeling and forecasting; 2435 Ionosphere: Ionospheric disturbances; 6974 Radio Science: Signal processing; 6982 Radio Science: Tomography and imaging; 6994 Radio Science: Instruments and techniques; *KEYWORDS:* GPS, Global Positioning System, ionosphere, TEC

Citation: Brunini, C., M. A. Van Zele, A. Meza, and M. Gende, Quiet and perturbed ionospheric representation according to the electron content from GPS signals, *J. Geophys. Res.*, *108*(A2), 1056, doi:10.1029/2002JA009346, 2003.

1. Introduction

[2] Although the Global Positioning System (GPS) was initially developed to serve as a radio navigation satellite system, it has become a powerful and mature geodetic tool today widely used for a broad range of technological and scientific applications. An extensive description of the system and how it works can be found in several classical text books, for example in the work of *Misra and Enge* [2001], among others. From the point of view of ionospheric studies, GPS represents the latest generation of satellite that may be used to study the ionosphere. Research studies on the matter can be traced back to the 1980s [e.g., *Kleusberg*, 1986; *Feess and Stephens*, 1987; *Lanyi and Roth*, 1988; *Wild et al.*, 1989] and were multiplied in the following years [e.g., *Coster et al.*, 1992; *Hajj et al.*, 1994; *Wilson et al.*, 1995; *Schaer et al.*, 1996; *Jakouski et al.*, 1996; *Davies and Hartmann*, 1997]. A detailed description about applications of GPS to ionospheric studies and a very comprehensive list of references is provided by *Manucci et al.* (A. J. Manucci, B. A. Iijima, U. J. Lindqwister, X. Pi, L. Sparks, and B. D. Wilson, GPS and ionosphere, revised submission to URSI reviews of *Radio Science*, Jet Propulsion Laboratory, Pasadena, Calif., March 1999, hereinafter referred to as Manucci et al., 1999). Many studies were focused on GPS observation analysis to study irregularities and perturbations in the ionosphere, including those caused by large geomagnetic storms [e.g., *Van Dierendonck et al.*, 1993; *Coco et al.*, 1995; *Coker et al.*, 1995; *Ho et al.*, 1996; *Aarons et al.*, 1997; *Pi et al.*, 1997; *Ho et al.*, 1998; *Afraimovich et al.*, 2000].

[3] Since the early 1990s, a worldwide network of permanent GPS tracking stations is rapidly growing up under the management of the International GPS Service (IGS) [*Beutler et al.*, 1999]. Even when this network was not planned for ionospheric studies, its observations have proved to be suitable for this purpose, providing continuous and quite good worldwide coverage at low cost for the users. In May 1998, IGS created the Ionosphere Working Group [*Feltens and Schaer*, 1998], and soon after five different centres started computing and making available several GPS-derived ionospheric products, mainly two-dimensional world-wide grids of vertical total electron content (VTEC) and differential code biases (DCBs) for

[1]Facultad de Ciencias Astronómicas y Geofísicas, Universidad Nacional de La Plata, La Plata, Argentina.
[2]Consejo Nacional de Investigaciones Científicas y Técnicas, Universidad de Buenos Aires, Buenos Aires, Argentina.
[3]Consejo Nacional de Investigaciones Científicas y Técnicas, Universidad Nacional de La Plata, La Plata, Argentina.

0148-0227/03/2002JA009346

every satellite and many receivers of the network. To make feasible interchanges and comparisons, the so-called IONEX (Ionosphere Map Exchange) standard format was established [*Schaer et al.*, 1998]. The five different centres that currently deliver VTEC maps to IGS are Jet Propulsion Laboratory (JPL) [*Manucci et al.*, 1998], European Space Agency (ESA) [*Feltens*, 1998], Centre for Orbit Determination in Europe (CODE) [*Schaer*, 1999], Universidad Politécnica de Cataluña (UPC) [*Hernández-Pajares et al.*, 1999], and Energy Mines and Resources of Canada (EMR). These use different algorithms to generate grids of VTEC with time resolution of at least 2 hours.

[4] In this paper, we use a very simple empirical global model to describe the distribution of the electron content integrated along the vertical path, from the Earth's surface up to the GPS satellites' height (VTEC). A set of parameters describes the distribution of the VTEC and DCBs for every satellite and every receiver. These are fitted on a daily basis using GPS observations from the IGS tracking network. Before being used, our model is compared with values computed by JPL and CODE IGS Analysis Centres, with VTEC values computed by the International Reference Ionosphere model (IRI-95) (D. Bilitza and K. Rawer, International Reference Ionosphere model (IRI-95), 1998. (Available as http://envnet.gsfc.nasa.gov/Models/EnviroNET_Models.html)), and with direct VTEC determinations provided by the Topex–Poseidon satellite [*Imel*, 1994]. Then we use our model to examine the global and seasonal morphology of the VTEC for selected quiet geomagnetic periods during the year 1997 (minimum solar activity and rising phase of the solar cycle 23) and to describe the largest scale disturbances of the VTEC during the biggest geomagnetic storm of that year, which occurred on May 15.

2. The GPS-Derived Ionospheric Model

[5] Dual frequency P-code GPS receivers such as those of the IGS tracking network can provide P-code and carrier phase measurements in both frequencies of the system, namely $f_1 = 1575.42$ MHz and $f_2 = 1227.60$ MHz. Forming ionospheric observable from the combination of the raw observations has been discussed in the literature [*Manucci et al.*, 1998; *Sardon and Zorraoa*, 1997; *Lanyi and Roth*, 1988]. Basically, when simultaneous carrier phase observations in both frequencies are subtracted, the satellite-receiver geometrical range and all frequency independent biases are removed and the so-called geometry-free linear combination, Φ_4, is obtained:

$$\Phi_4 = \Phi_1 - \Phi_2 = -k\mathrm{STEC} + C_R + C^S + C_R^S + \varepsilon \qquad (1)$$

where Φ_1 and Φ_2 are the raw carrier phase observations in both frequencies, k is a constant, STEC is the slant total electron content (the electron content integrated along the slant path of the signal form the receiver to the satellite), C_R and C^S are the so-called differential code biases (DCBs) due to electronic delays produced in the hardware of the receiver and the satellite, respectively; C_R^S is a constant related with the carrier phase ambiguities in both frequencies; and ε is the resultant measurement error.

[6] Before being used, we do a preprocessing of the raw observations to detect jumps in the carrier phase observations. We estimate a C_R^S value for every continuous arc, averaging the differences between carrier phase and P-code observations, and then this value is subtracted from the carrier-phase observations. In this way, every continuous arc of carrier phase observations is "levelled" (on an average) to the P-code observations and the ambiguities are removed from the problem.

[7] Since we are not interested in the study of rapid variations, we decide to condense the raw data in normal points every 8 min. This task is performed at the preprocessing stage. We group the raw data in adjacent intervals of 8 min and 16 data per interval for the usual 30-s sampling rate of the IGS receivers and fit a straight line by least squares for every interval. We obtain the normal points by evaluating the linear approximation at the middle point of each interval. The main criterion for the choice of 8 min and linear approximation was to minimize the bias between normal points and raw data.

[8] DCBs for both receivers and satellites remain as unknowns and we estimate daily constant values together with the sought ionospheric information. There are evidences that satellite DCBs are quite stable for period of several months [*Coco et al.*, 1991; *Wilson and Manucci*, 1994; *Sardon and Zarraoa*, 1997]. The stability of the receivers DCBs is more complicated to assess. Calibration for most receivers of the IGS network is performed once per day and we followed the same criterion in this work. The stability of our daily estimate DCBs will be addressed in the next section.

[9] We adopted the early but still common "shell-ionosphere" model [*Manucci et al.*, 1999]. The central approximation of this model is to assume that there are no horizontal variations of the electron distribution along the ray path of the signal from satellite to receiver. This approximation may worsen for low-elevation observations, particularly during dusk local times or in the equatorial regions. We assume that the overall electron content is concentrated in an infinitesimal thin shell located close to the height where the ionosondes detect the higher electron density, namely the F2 region. We adopted the widely used "thin shell" obliquity factor, M [*Lanyi and Roth*, 1988; *Coco et al.*, 1991; *Wilson et al.*, 1995] to relate slant and vertical TEC:

$$M = \frac{\mathrm{STEC}}{\mathrm{VTEC}} \cong \left[\sqrt{1 - \frac{R}{R+H}\cos(E)}\right] \qquad (2)$$

where E is the elevation angle of the satellite, R is the mean radius of the Earth, and H is the height of the shell. To determine this height, we used the IRI-95 model [*Komjathy et al.*, 1998]. A low order spherical harmonic expansion which depends on the geographical latitude and local time was fitted to the F2 layer height given by the IRI-95. The obtained heights vary between 250 and 306 km for different geographical regions and dates during the year 1997.

[10] To describe the spatial distribution of the VTEC over the shell, we adopted the so-called "Sun-fixed" geographic co-ordinate system, which rotates around the *Z axis* synchronically with the Sun. It is assumed that the use of this system reduces the UT-variability of the ionosphere [*Wilson*

et al., 1995]. The distribution of the VTEC over the shell is represented with a spherical harmonics expansion up to a maximum degree and order equal to 12 and 8, respectively [*Schaer*, 1999]:

$$\mathrm{VTEC}(h,\phi) = \sum_{l=0}^{12} \sum_{m=0}^{l\le 8} \left\{ a_{lm} \cos\left(2\pi \frac{mh}{24}\right) + b_{lm} \sin\left(2\pi \frac{mh}{24}\right) \right\} P_{lm}(\sin\phi) \quad (3)$$

where h and ϕ are the spherical co-ordinates in the Sun-fixed geographic system, $P_{lm}(\sin\phi)$ is the Legendre-associated function, and a_{lm} and b_{lm} are the expansion coefficients which we fit using the GPS observations.

[11] Replacing equations (2) and (3) in equation (1) and operating allows us to establish equation (4), which links the observations and the unknowns, and is the equation of observation for the problem:

$$\Phi_4 - C_{\mathrm{R}}^{\mathrm{S}} - \varepsilon = -kM\mathrm{VTEC}(a_{lm}, b_{lm}) + C_{\mathrm{R}} + C^{\mathrm{S}} \quad (4)$$

We use observations from 63 to 76 IGS stations (taken from anonymous ftp from lox.ucsd.edu) to estimate the unknowns by least squares. The criterion to select the site was to achieve a worldwide coverage of observation as homogeneous as possible. In spite of that, large hole (mainly over ocean regions) were insurmountable. As a counterpart, we select a few representative stations in those regions where dense tracking networks exist (USA, Europe). We process the observations on a daily basis: we estimate independent DCBs for every day and a set of spherical harmonics expansion coefficients for every 2-hour UT intervals [0–2), [2–4), ..., [22–24). We use the estimated coefficients to compute VTEC maps, some of which are shown in the following sections. These maps also show the location of the observing stations that participated in the corresponding VTEC estimation.

[12] Spherical harmonics global VTEC maps with 2-hour time resolution are routinely produced by CODE [*Schaer*, 1999] and delivered to IGS. Maps with 6- and 12-hour time resolution were first computed at JPL in 1993 and shown to be quite accurate in the midlatitudes [*Wilson et al.*, 1995]. The midlatitude ionosphere is smoother and less variable than the equatorial region, so averaging over time and effectively shifting the data into longitude to fill in a global map, turn out to be effective. The use of spherical harmonics and the Sun-fixed system is less effective in the equatorial region. In 1994, JPL began using a local basis set (bicubic splines on the sphere), the solar-geomagnetic co-ordinate system and Kalman filtering with stochastic parameters to increase the spatial resolution to about 5° and time resolution to 15 min (using 100 GPS sites). Using dense regional networks of GPS receivers, a modification of this algorithm has been employed to obtain VTEC maps in the continental USA and Europe with 3° spatial resolution and 5-min time resolution [*Manucci et al.,* 1999].

[13] Later in this paper, we will focus on the analyses of large-scale spatial ionospheric structures during quiet and disturbed time, and the evolution of the overall VTEC level (related with the a_{00} coefficient of the spherical harmonic expansion) during the year 1997. The following section is devoted to validate our results by means of comparisons with GPS-independent ionospheric results and GPS-derived VTEC computed by other research groups.

3. Validation of the GPS-Derived VTEC

[14] We have compared our VTEC estimates (hereafter named LPIM) with GPS-independent estimates computed using the International Reference Ionosphere (IRI-95) and provided by the Topex-Poseidon satellite, and with GPS-derived VTEC values delivered to IGS by CODE and JPL.

[15] IRI-95 provides averages values in the nonauroral ionosphere for magnetically quiet conditions (D. Bilitza and K. Rawer, International Reference Ionosphere model (IRI-95), 1998. (Available as http://envnet.gsfc.nasa.gov/Models/EnviroNET_Models.html)). Topex provides, through its onboard double-frequency altimeter, a direct VTEC determination for any geographic longitude and latitudes between ±66° [*Imel*, 1994]. The noise of Topex determinations is reduced substantially at about ±1 TECU by averaging the data over 20 s (total electron content unity, TECU = 10^{16} electron/m^2). The uncertainly in VTEC is dominated by uncertainly in the so-called electromagnetic bias, due to the difference in reflectivity of wave troughs versus wave peaks, and to certain assumptions made in the on board algorithm. This bias has been partially compensated in the Generation B data by adding a bias to the C-band range delay before differencing the C and K_{u}-band range delays to obtain VTEC. Nevertheless, it is believed that there remains a bias of about +2 to +4 TECU in the Topex-derived VTEC [*Codrescu et al.*, 2001]. Topex is sensitive to the ionosphere up to about 1330 km, and so the higher protonosphere is not sensed. This contribution is not included either in the VTEC computed with IRI-95 but, up to some extent, it is present in the GPS VTEC estimation and may produce, therefore, a negative bias between GPS and IRI or TOPEX. It is believed, however, that this bias does not exceed by a few TECU.

[16] We have compared the VTEC estimates obtained using LPIM with those obtained by IRI-95 and Topex measurements [*Meza et al.*, 2002]. We worked with three 10-day Topex cycles during the year 1997, namely cycles, 175 (days 165–171 during June solstice), 187 (days 286–295, October equinox), and 194 (days 354–363, December solstice). During these periods, the geomagnetic conditions (measured by the K_{m} index [*Menvielle and Berthelier*, 1991]) stayed quiet, and therefore IRI-95 is suitable to represent the ionospheric conditions. In conclusion, we can say that our model predominantly underestimates the VTEC with respect to Topex. The global average difference ranges from −2.5 to −2.9 TECU. This lies well within the range of bias values determined for other GPS ionospheric models [*Ruffini et al.*, 1998 and references therein]. Figure 1a shows the differences for October equinox. The differences LPIM-IRI exhibit a stronger dependency with time and especially with latitude. Their global average ranges from −1.6 to +1.9 TECU.

[17] The comparisons with Topex reveal that IRI and LPIM characterize the VTEC at midnorthern latitudes better than at midsouthern latitudes. The reason could be that data used to perform IRI come from network of

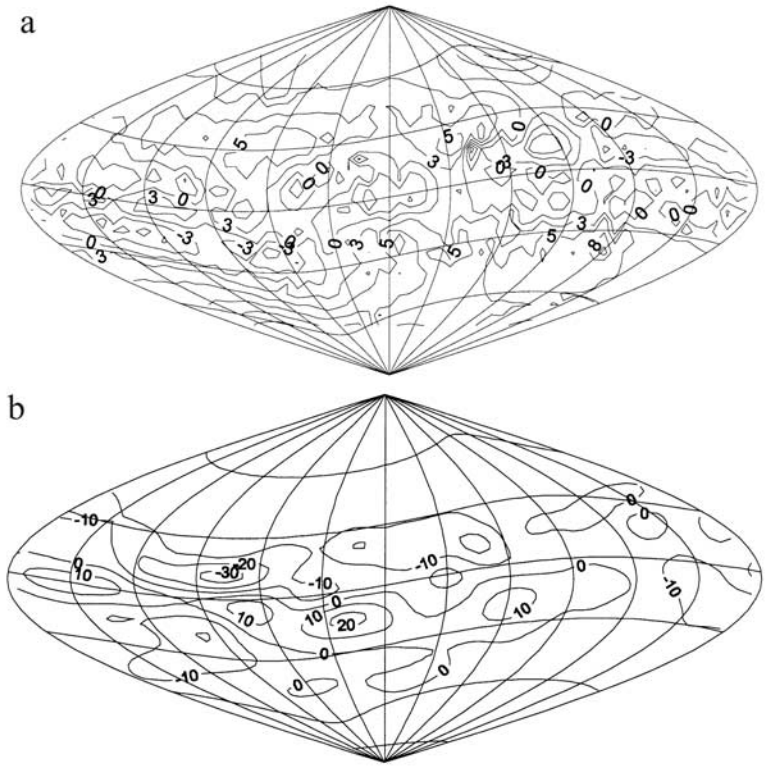

Figure 1. (a) LPIM-Topex VTEC differences for a 10-day Topex cycle. (b) LPIM-JPL VTEC differences; the figure shows the largest differences we found, happened for the interval [0−2) UT during the large 9 September 1999 geomagnetic storm. The co-ordinates are geographic longitude and geomagnetic latitude in sinusoidal projection; VTEC values are in TECU.

ionosondes and incoherent scatter measurements placed mostly at the North Hemisphere. Similarly, the measurements used to perform LPIM come from GPS receivers better distributed at the North Hemisphere. The largest differences tend to appear in the equatorial region. During June solstice, the differences at northern and southern midlatitude are similar but during December solstice are clearly larger at the southern midlatitude. The largest differences appear during October equinox. The analysis of this limited sample suggest that added to the problem of data coverage, there are worse model representations in the region where the Sun is placed.

[18] Following our analysis, we compared our VTEC with the corresponding values delivered to IGS by CODE and JPL. Comparisons were made for the days 248, 249 264, 265, 266, 267 and 268 of the year 1999, during which the geomagnetic conditions vary from very quiet to very disturbed. Particularly, during the days 265−266, the largest geomagnetic storm of the year 1999 took place. The global average difference is −1.0 TECU for LPIM-CODE and −4.8 TECU for LPIM-JPL. The following global average differences between VTEC estimated by different IGS Ionosphere Analysis Centres were found by *Schaer* [1999]: −4.6 TECU for COD-JPL, −3.7 TECU for EMR-JPL, −5.0 for ESA-JPL, and −3.2 for UPC-JPL. We conclude, therefore, that the overall level of our estimation (related with the a_{00} coefficient of the spherical harmonics expansion in equation (3)) is in agreement with the values estimated by other research groups.

[19] We found that the discrepancies worsen about 50% during the main and the recovery phase of the storm with respect to the starting phase of the storm or the quiet intervals. The largest discrepancies take place in the regions with highest electron content and tend to enlarge for those 2-hour intervals in which this condition occurs over ocean areas with poor data coverage. Figure 1b shows a map of the largest discrepancies found, happened between LPIM and JPL, for the interval [0, 2) UT of the day 266, during the main phase of the geomagnetic storm. The largest differences shown in this map represent about 30% of the corresponding VTEC.

[20] Finally, we compared for the same periods our DCBs with those of CODE and JPL. The RMS difference between LPIM and JPL for the satellite is ±0.9 TECU. The corresponding value for the differences between LPIM and CODE is ±0.5 TECU. Discrepancies are large for the receivers: the corresponding RMS differences are ±3.1 TECU for LPIM-JPL and ±1.5 TECU for LPIM-CODE. The daily repeatability of our DCBs along the year 1997 (excluding storm times) is ±0.4 TECU (rms) for satellites and ±2.4 TECU (rms) for receivers.

[21] From the preceding analysis, we conclude that our solutions for the GPS instrumental biases are reasonable and, therefore, the level of the absolute slant TEC we are computing from GPS data is also reasonable. Our VTEC maps are suitable to detect large-scale features in the VTEC distribution, but we have to take account of the artificial representation of the VTEC maps in regions

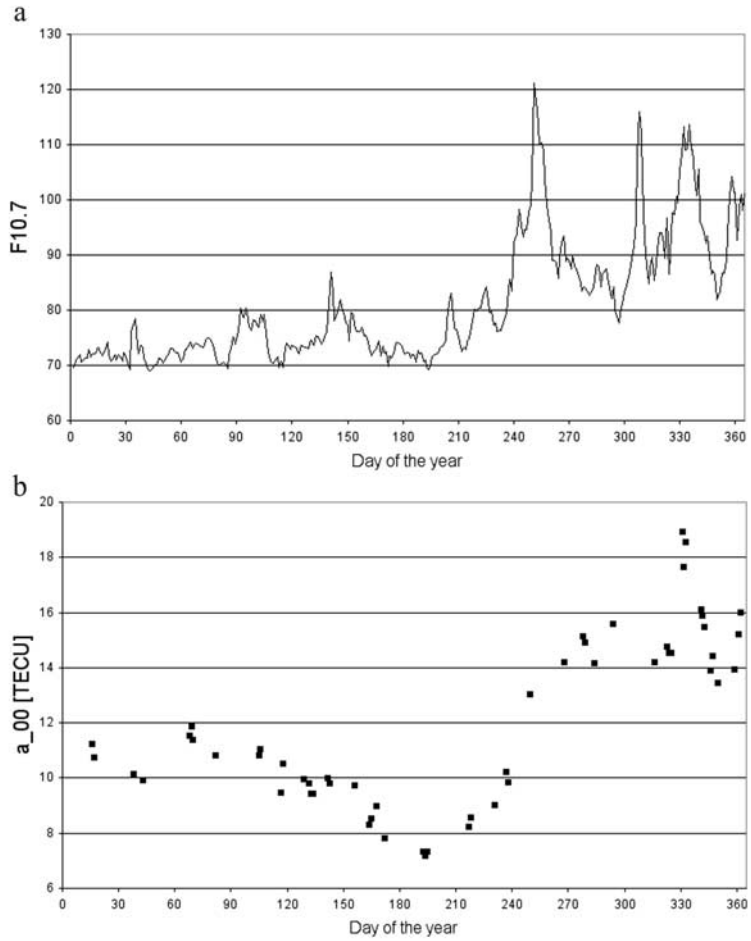

Figure 2. (a) F10.7 solar flux daily index. (b) a_{00} Coefficient of the spherical harmonic expansion for quiet geomagnetic days. (c) Daily sunspot Wolf number, during the year 1997.

where data coverage is not good, especially during geomagnetic storm.

4. Results

4.1. VTEC During Quiet Geomagnetic Periods

[22] As a measure of the ionospheric perturbation, we used the geomagnetic activity indexes K_m [*Menvielle and Berthelier*, 1991], which are related to the midenergy density imbedded in the irregular magnetic variations at midlatitudes. Chosen intervals with low values of K_m allow us to assume that the solar radiation is the only energy source responsible for the regular ionization taking place at the high atmosphere. We consider [0–2), [2–4),. . ., [22–24) UT intervals whose K_m indices are lower than 1+.

[23] More than 800 2-hour intervals have been fitted to analyze quiet VTEC variation along the year 1997. In the following statements, we summarize some macroscopic behavior, which can be extracted from the analysis of the variation of the a_{00} and a_{10} coefficients (equation (3)).

[24] The variation of the a_{00} coefficient is approximately proportional to the global average VTEC and is represented in Figure 2b (every point represents the average of all quiet 2-hour intervals in each day). The correlation of VTEC (ρ = 0.86) with the intensity of the solar flux measured by the F10.7 daily index (Solar Geophysical Data, prompt reports, 641, (part 1), January 1998), represented in Figure 2a, is quite evident. A lower correlation (ρ = 0.62) was noted with the daily sunspot Wolf number, represented in Figure 2c.

[25] The variation of the a_{10} coefficient, which measures the North-South bias of global VTEC distribution, shows a strong correlation (ρ = 0.97) with the declination of the Sun.

[26] If the period from January 1 to August 27 (days 1–239) is considered, during which F10.7 remains approximately constant, the global averaged VTEC (Figure 2b) is greater in January than in June. This result is in agreement with independent observations of F2 electron density, which shows that during the day the values for December are greater than those for June by about 20% [*Hargreaves*, 1992] and that the values measured at noon, between 50° North and 35° South, are greater in December than in June [*Ratcliffe and Weekes*, 1960].

[27] During the period of approximately constant solar flux, the maximum global-averaged VTEC takes place at March equinox (day 80) in accordance with the semi-annual anomaly of the F2 layer [*Hargreaves*, 1992]. The behavior at the September equinox is hidden by the large increase in the solar flux.

[28] Figures 3a–3d show some selected global 2-hour VTEC maps. The main conclusions extracted from the analysis of a large number of maps similar to those presented in these figures are summarized below.

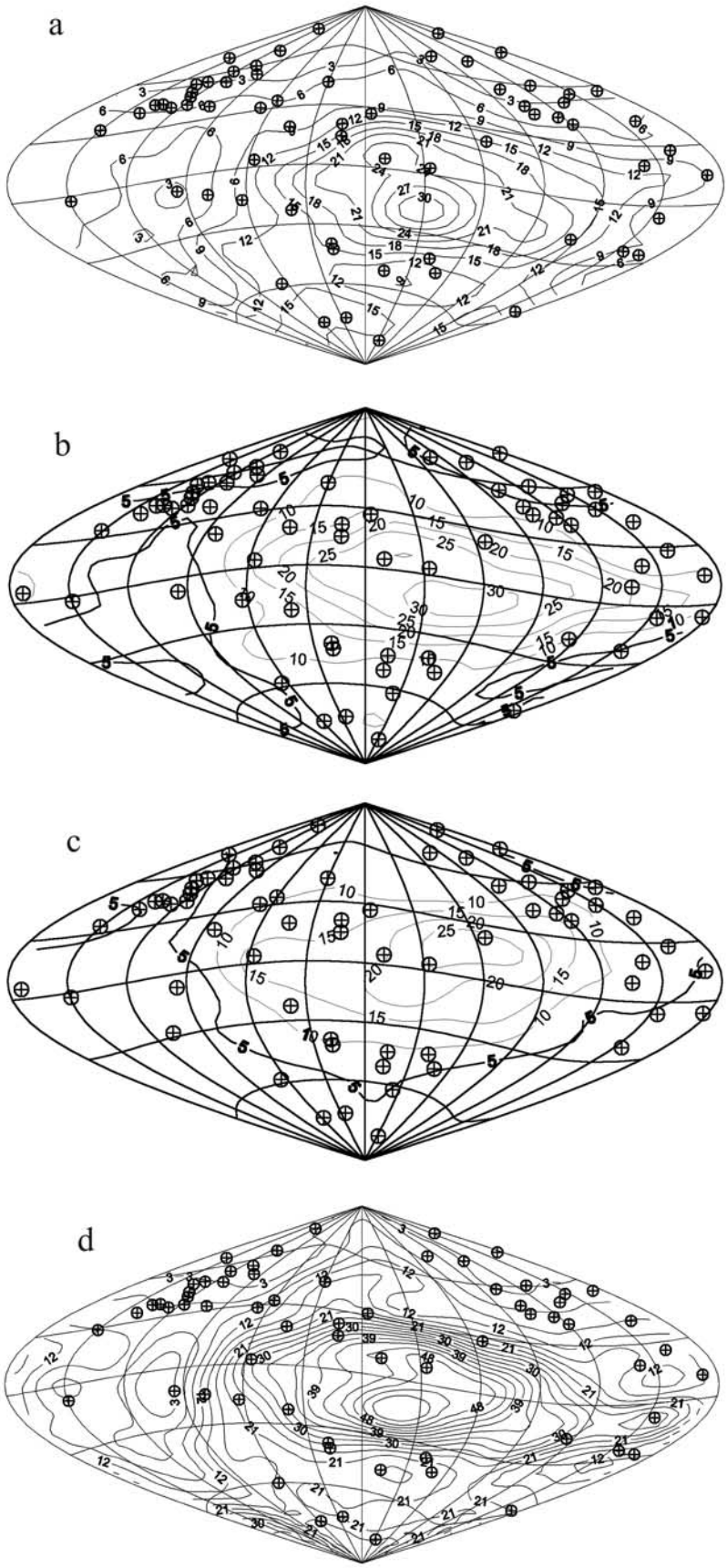
a
b
c
d

Table 1a. a_{00} Coefficients (in TECU) of the VTEC Expansion for 2-Hour Quiet Intervals Along Five Days Close to the Storm and With Similar Solar Activity

Interval	MAY 9 *F10.7 = 73.0*	MAY 12 *73.7*	MAY 13 *75.4*	MAY 23 *78.1*	JUN 5 *76.1*	Average	Std. Dev.
[0–2)	10.5	9.77	9.17	9.78	9.77	9.80	±0.47
[2–4)	10.61	9.76	9.2	9.84	10.07	9.90	±0.51
[4–6)	10.85	9.92	9.29	10.2	10.41	10.13	±0.58
[6–8)	10.96	10.05	9.34	10.09	10.23	10.13	±0.58
[8–10)	10.74	9.83	9.22	10.01	9.9	9.94	±0.54
[10–12)	10.61	9.55	9.28	9.74	9.51	9.74	±0.51
[12–14)	10.29	9.56	9.48	9.46	9.17	9.59	±0.42
[14–16)	9.78	9.69	9.53	9.45	9.11	9.51	±0.26
[16–18)	9.74	9.8	9.64	9.68	9.16	9.60	±0.26
[18–20)	9.89	9.8	9.59	9.79	9.29	9.67	±0.24
[20–22)	9.99	9.81	9.54	9.9	9.52	9.75	±0.21
[22–24)	9.91	9.89	9.2	10.15	9.61	9.75	±0.36

Table 1b. a_{00} Coefficients (in TECU) of the VTEC Expansion for the 2-Hour Intervals Covering the Storm (Left Columns) and "Sigma-Event" Levels (Right Colums)

Interval	MAY 14 *F10.7 = 75.1*		MAY 15 *74.7*		MAY 16 *73.9*	
[0–2)	9.27	−1.12	10.77	2.06	8.02	−3.77
[2–4)	9.37	−1.03	11.31	2.76	7.72	−4.25
[4–6)	9.51	−1.07	12.16	3.49	7.89	−3.86
[6–8)	9.52	−1.06	13.16	5.25	8.17	−3.40
[8–10)	9.44	−0.92	13.25	6.10	8.16	−3.28
[10–12)	9.26	−0.93	12.92	6.19	8.37	−2.66
[12–14)	9.24	−0.84	11.99	5.75	8.8	−1.90
[14–16)	9.32	−0.74	11.38	7.20	9.31	−0.78
[16–18)	9.6	−0.02	10.78	4.60	9.73	0.49
[18–20)	9.89	0.91	9.79	0.49	9.65	−0.09
[20–22)	10.22	2.20	8.9	−4.01	9.3	−2.13
[22–24)	10.54	2.17	8.3	−4.00	9.17	−1.60

[29] In agreement with the F2 behavior [*Hargreaves*, 1992], VTEC distribution does not have a pattern which repeats itself in quiet days.

[30] Maximum VTEC happens between 14 and 18 hours (local time) independently of the epoch of the year. VTEC distribution is not symmetric and is shifted from the noon meridian toward afternoon, showing that the rate of electron loss at noon is lower than the rate of production by solar photo-ionization, during this year of low solar activity. This is in agreement with results extracted from ionosonde observations, which show that during low solar activity the maximum electron content in the F2 region does not take place often at noon, as usual in the E region, but in the afternoon [*Van Zandt*, 1967; *Hargreaves*, 1992].

[31] VTEC at about 30° of latitude in the summer hemisphere does not vanish after sunset, and even during night, extending sometime up to sunrise. This resembles the F2 behavior likely due to the dependence between the rate of reaction of the interchange of charges and the temperature (low loss rate) [*Van Zandt*, 1967; *Hargreaves*, 1992].

[32] If the period of approximately constant solar flux is considered, noon VTEC values are greater in the summer than in the winter hemisphere. During the equinox, it can be seen (Figure 3b) that: (a) VTEC reaches its maximum in equatorial latitudes; (b) VTEC is minimum between 50° and 90° of latitude in the shadow hemisphere; and (c) in the equatorial region VTEC is minimum between 1 and 5 hours (local time).

[33] During the solstices (Figures 3a, 3c, and 3d), it is evident that (a) VTEC reaches its maximum in the summer hemisphere, (b) in the winter hemisphere, VTEC is minimum between about 80° at noon and 50° at midnight; (c) in the equatorial region, VTEC is minimum between 21 and 7 hours (local time); and (d) in spite of the greater detail, the pattern of Figure 3d is similar to the pattern of Figure 3a.

4.2. VTEC During the May 15, 1997 Geomagnetic Storm

[34] As the provisional equatorial Dst and the provisional auroral AU and AL indexes show, the 15 May 1997 storm was the result of intensification of the auroral electrojets and ring current. Table 1a shows the a_{00} coefficients of the VTEC expansion (equation (3)) for the 2-hour quiet intervals of 5 days close to the storm and with similar solar activity. From these values, we computed quiet averages and quiet standard deviations. These values are assumed as representative of the quiet overall VTEC and the quiet variability of the corresponding 2-hour interval. Table 1b shows the a_{00} coefficient for the 2-hour intervals covering the storm period. From both tables, we computed the differences between the a_{00} for the storm and the corresponding quiet averages, and then, the ratio of these differences to the corresponding standard deviations. This ratio is used to characterize the impact of the storm over the overall VTEC as a 2, 3, and so on sigma-event. These "sigma-events" are shown in Table 1b and have been represented in Figure 4a. Several geomagnetic indexes have also been represented in the Figure 4 [*Mayaud*, 1980]: the provisional Dst index (Bulletin Mensuel No 97-5, Bureau des Publications SIIG, WDC-C2), expression of the ring equatorial current (Figure 4b); the Am index (Bulletin No 97-5, Bureau des Publications SIIG, WDC-C2), expression of the geomagnetic activity at mean latitudes (Figure 4c); and the AL and AU indexes http://swdcdb.kugi.kyoto-u.ac.jp/aedir/ae1/q/AEyear1997.html), expressions of the intensity of the auroral electrojets (Figure 4d). Finally, Figures 5a to 6c show global VTEC maps for six selected 2-hour intervals covering the development of the storm. The outstanding features observed in Figures 4–6 are summarized in the following statements: the overall VTEC starts increasing simultaneously with the auroral indexes AU and AL and approximately 9 hours before that the Dst index shows the initial phase of the storm; the overall VTEC reaches its maximum between 9 and 15 hours UT, simultaneously with the auroral activity; at the same time, the maximum electron content shifts from North to South and the main phase of the storm takes place; during the main phase of the storm, the maxima of the VTEC distribution (located close to the geomagnetic equator) become blurred; when the geomagnetic storm is going

Figure 3. (opposite) Typical VTEC global maps for 2-hour quiet geomagnetic periods: (a) [0–2) UT of 17 January 1997 (close to December solstice, F10.7 = 71.7); (b) [0–2) UT of 23 March 1997 (close to March equinox, F10.7 = 70.3); (c) [0–2) UT of 21 June 21 1997 (close to June solstice, F10.7 = 69.8); (d) [0–2) UT of 28 November 1997 (close to December solstice, F10.7 = 113.2). The co-ordinates are Sun-fixed longitude and geomagnetic latitude in sinusoidal projection; values are in TECU; circled plus symbols represent the average location of the observing stations.

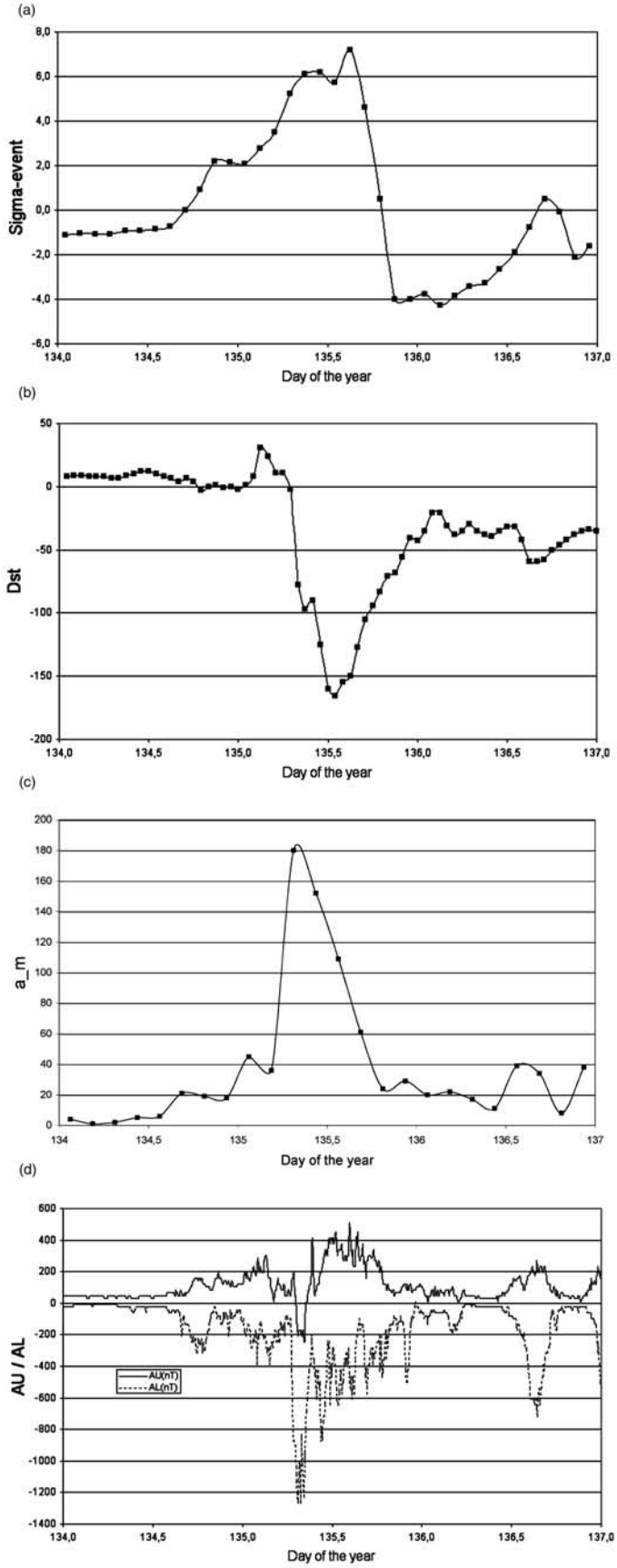

Figure 4. (a) "Sigma-events" for the 15 May 1997 (Day 135) geomagnetic storm. (b) AM geomagnetic index. (c) Provisional Dst geomagnetic index. (d) Auroral AU and AL geomagnetic indexes.

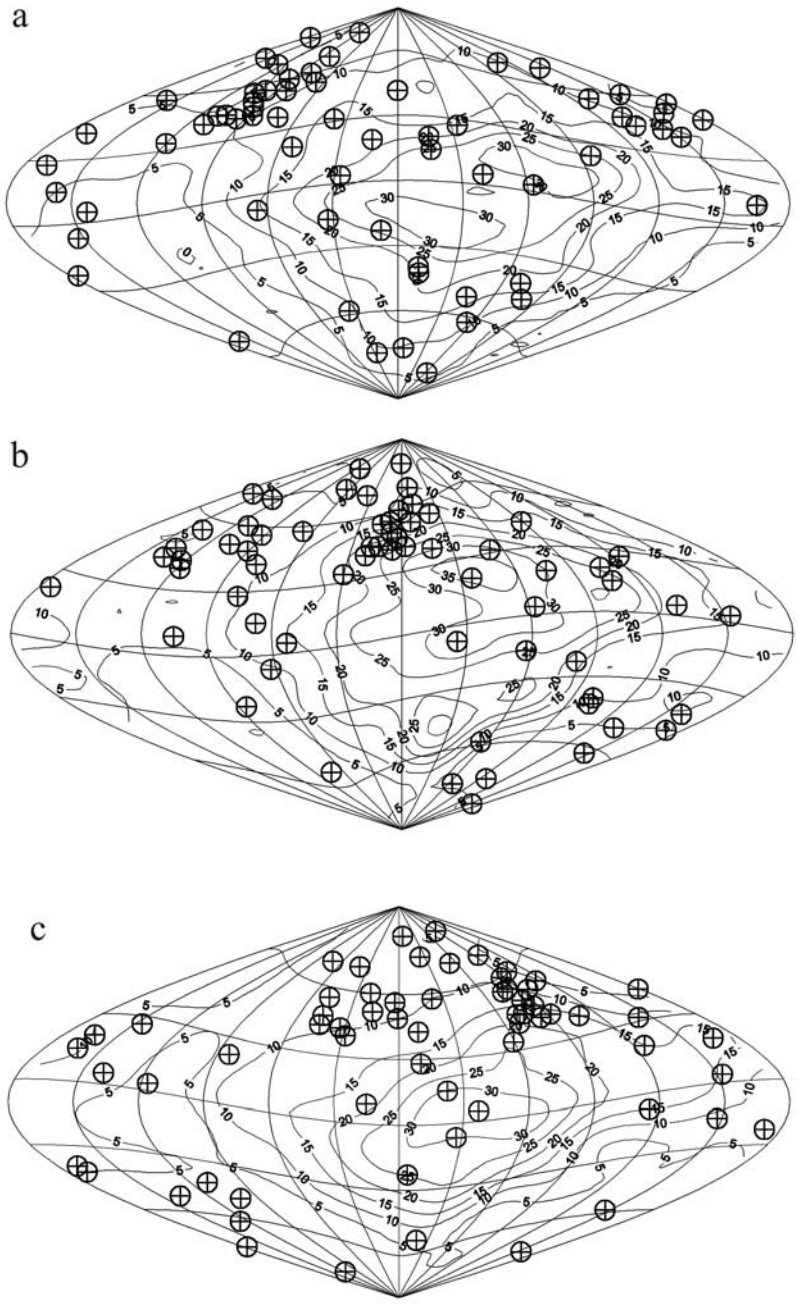

Figure 5. Selected VTEC global maps for 2-hour intervals during the main phase of the 15 May 1997 geomagnetic storm. (a) [4–6) UT of 15 May. (b) [10–12) UT of 15 May. (c) [16–18) UT of 15 May. The co-ordinates are Sun-fixed longitude and geomagnetic latitude in sinusoidal projection; values are in TECU; circled plus symbols represent the average location of the observing stations.

into its recovery phase, a fast decreasing of the overall VTEC takes place while the auroral activity decreases; low values of VTEC persist during the recovery phase of the storm; the overall VTEC reaches its minimum between 21 UT of the day 135 (May 15) and 9 UT of the day 136 (May 16), while a decreasing of the electron content that started at midlatitudes in the North Hemisphere expanded over midlatitudes in both hemispheres; during the recovery phase of the storm, the maximum electron content moves from its typical location during quiet days and a large decreasing takes place; and the later increasing in the overall VTEC is related with a second intensification of the auroral electrojects.

[35] The precedent behaviors suggest that the variation of the electron content differs significantly from the values observed during quiet geomagnetic periods when the auroral indexes show a perturbation.

5. Conclusions and Further Work

[36] The results presented in this paper show that, during quiet geomagnetic periods and low solar activity, GPS

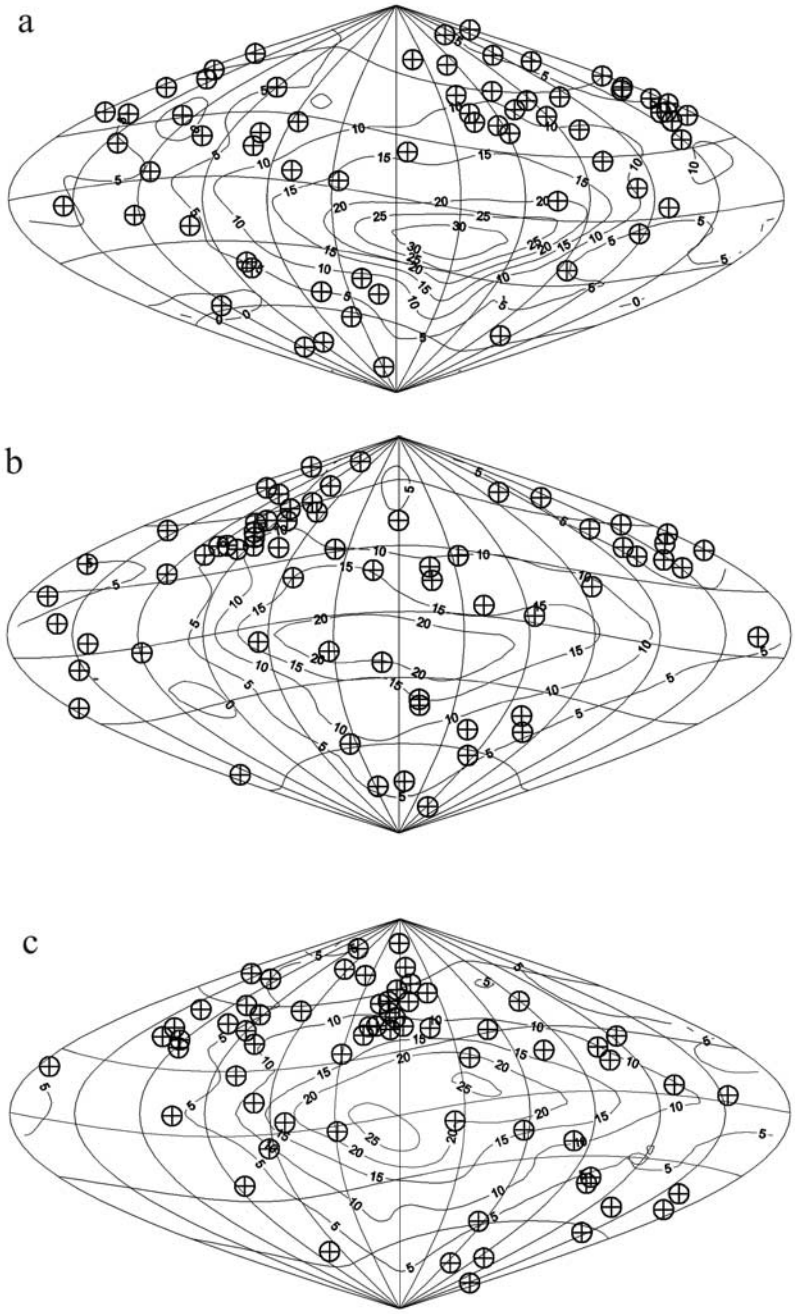

Figure 6. Selected VTEC global maps for 2-hour intervals during the recovery phase of the 15 May 1997 geomagnetic storm. (a) [22–24) UT of 15 May. (b) [4–6) UT of 16 May. (c) [10–12) UT of 16 May. The co-ordinates are Sun-fixed longitude and geomagnetic latitude in sinusoidal projection; values are in TECU; circled plus symbols represent the average location of the observing stations.

observations can provide a global visualization of the electron content integrated from the Earth's surface up to height of about 22,000 km, describing most of the large-scale features of the F2 ionospheric layer, as well as the time evolution with a resolution of at least 2 hours. Even when a higher time resolution would be desirable to follow the ionospheric dynamics during a geomagnetic storm, the results obtained studying the 15 May 1997 storm are encouraging and show the capability of identifying large-scale storm features.

[37] Even when the current geographical coverage of the ground base tracking GPS network limits the spatial and time resolution of the ionospheric global models, GPS represents an unprecedented opportunity for ionospheric scientists, since its observations provide almost global coverage with simultaneity and time continuity, at low cost for the users and are readily accessible. In spite of the fact that the rather simple empirical model that we have used to fit the observations must be improved, we believe that GPS global ionospheric maps are of great help for a better understanding of the complex ionospheric environment (mainly the F2 region) and the global response of the ionosphere to geomagnetic storms.

[38] There is plenty of effort in processing GPS data to form VTEC maps, but we believe that less effort is currently spent on their validation and interpretation. Daily VTEC maps with 15-min resolution from JPL are available since 1995 and global maps with 2-hour resolution, submitted by five IGS Ionospheric Analysis Centres, are available in IONEX format, for at least the last 2 years. In a further work, we will try to combine them with other ionospheric data to study global ionospheric climatology and global ionospheric response to geomagnetic storms.

[39] **Acknowledgments.** We wish to thank W. Bosch from the Deutsches Geodätisches Forschungsinstitut who provided us the Topex data; the Institute of Geophysics and Planetary Physics, the World Data Centre for Geomagnetism, the Fédération des Services d'Analyse de Données Astronomiques et Geophysiques, and the Scripps Institution of Oceanography from the University of California, San Diego, for the free availability of geomagnetic indexes and GPS data. The National Space Science Data Centre, where the IRI software is available is also thanked. Last, but not least, we wish to acknowledge the reviewers for their very fruitful comments and suggestions to improve this paper.

[40] Arthur Richmond thanks Cemil Erol and Brian D. Wilson for their assistance in evaluating this paper.

References

Aarons, J., M. Mendillo, and R. Yantosca, GPS phase fluctuations in the equatorial region during sunspot minimum, *Radio Sci.*, *32*(4), 1535–1550, 1997.

Afraimovich, E. L., A. T. Altyntsev, E. A. Kosogorov, N. S. Larina, and L. A. Leonovich, Ionospheric effects of the solar flares of September 23, 1998 and July 29, 1999 as deduced from global GPS network data, *J. Atmos. Sol. Terr. Phys.*, *63*(17), 1841–1849, 2000.

Beutler, G., M. Rothacher, S. Schaer, T. A. Springer, J. Kouba, and R. E. Neilan, The International GPS Service (IGS): An interdisciplinary service in support of the Earth sciences, *Adv. Space Res.*, *23*(4), 631–635, 1999.

Coco, D. S., C. Coker, S. R. Dahlke, and J. R. Clynch, Variability of GPS satellite differential group delays biases, *IEEE Trans. Aerosp. Electron. Syst.*, *27*, 931–938, 1991.

Coco, D. S., T. L. Gaussiran, and C. Coker, Passive detection of sporadic-E using GPS phase measurements, *Radio Sci.*, *30*(6), 1869–1874, 1995.

Codrescu, M. V., K. L. Beierle, T. J. Fuller-Rowell, S. E. Palo, and X. Zhang, More total electron content climatilogy from Topex/Poseidon measurements, *Radio Sci.*, *36*(2), 325–333, 2001.

Coker, C., R. Hunsucker, and G. Lott, Detection of auroral activity using GPS satellites, *Geophys. Res. Lett.*, *22*(23), 3259–3262, 1995.

Coster, A. J., E. M. Gaposchkin, and L. E. Thorton, Real-time ionospheric monitoring system using the GPS, *Navigation*, *39*, 191–204, 1992.

Davies, K., and G. K. Hartmann, Studying the ionosphere with the Global Positioning System, *Radio Sci.*, *32*(4), 1695–1703, 1997.

Feess, W. A., and S. G. Stephens, Evaluation of GPS ionospheric time delay model, *IEEE Trans. Aerosp. Electron. Syst.*, *23*(3), 332–338, 1987.

Feltens, J., Chapman profile approach for 3-d global TEC representation, in *Proceedings of the IGS Analysis Center Workshop*, edited by J. M. Dow, J. Kouba, and T. Springer, pp. 285–297, Darmstadt, February 9–11, 1998.

Feltens, J., and S. Schaer, IGS Products for the Ionosphere, in *Proceedings of the IGS Analysis Center Workshop*, edited by J. M. Dow, J. Kouba, and T. Springer, pp. 225–232, Darmstadt, February 9–11, 1998.

Hajj, G. A., R. Ibañez-Meier, E. R. Kursinski, and L. J. Romans, Imaging the ionosphere with the Global Positioning System, *Int. J. Imaging Syst. Technol.*, *5*(2), 174–178, 1994.

Hargreaves, J. K., The solar-terrestrial environment, in *Cambridge Atmospheric and Space Science Series*, pp. 228–255, Cambridge Univ. Press, New York, 1992.

Hernández-Pajares, M., J. M. Juan, and J. Sanz, New approaches in global ionospheric determination using ground GPS data, *J. Atmos. Sol. Terr. Phys.*, *61*, 1237–1247, 1999.

Ho, C. M., A. J. Manucci, U. J. Lindqwister, X. Pi, and B. T. Tsurutani, Global ionospheric perturbations monitored by the worldwide GPS network, *Geophys. Res. Lett.*, *23*, 3219–3222, 1996.

Ho, C. M., A. J. Mannucci, L. Sparks, X. Pi, U. J. Lindqwister, B. D. Wilson, B. A. Iijima, and M. J. Reyes, Ionospheric total electron content perturbations monitored by the GPS global network during two northern hemisphere winter storms, *J. Geophys. Res.*, *103*(A11), 26,409–26,420, 1998.

Imel, D. A., Evaluation of the Topex/Poseidon dual-frequency ionosphere correction, *J. Geophys. Res.*, *99*(C12), 24,895–24,906, 1994.

Jakouski, N., E. Sardon, E. Egler, A. Jungst, and D. Klahn, About the use of GPS measurements for ionospheric studies, in *GPS Trends in Precise Terrestrial Airborne and Spaceborne Applications, IAG Symposium 115*, edited by G. Beutler et al., Springer-Verlag, New York, 1996.

Kleusberg, A., Ionospheric propagation effects in geodetic relative GPS positioning, *Manuscr. Geod.*, *11*, 256–261, 1986.

Komjathy, A., R. B. Langley, and D. Bilitza, Ingesting GPS-derived TEC data into the International Reference Ionosphere for single frequency radar altimeter ionospheric delay corrections, *Adv. Space Res.*, *22*(6), 792–801, 1998.

Lanyi, G. E., and T. Roth, A comparison of mapped and measured total ionospheric electron content using Global Positioning System and beacon satellite observations, *Radio Sci.*, *23*(4), 483–492, 1988.

Manucci, A. J., B. D. Wilson, D. N. Yuan, C. M. Ho, U. J. Lindqwister, and T. F. Runge, A global mapping technique for GPS-derived ionospheric total electron-content measurements, *Radio Sci.*, *33*(3), 565–582, 1998.

Mayaud, P. N., Deviation, meaning and use of geomagnetic indices, *AGU Geophys. Mongr.*, *22*, 1980.

Menvielle, M., and A. Berthelier, The K-derived planetary indices: Description and availability, *Rev. Geophys.*, *29*(3), 415–432 (See also *30*(1), 91), 1991.

Meza, A., C. Brunini, W. Bosch, and A. Van Zele, Comparing vertical total electron content from GPS, Bentt and IRI models with TOPEX-POSEIDON, *Adv. Space Res.*, *30*(2), 307–312, 2002.

Misra, P., and P. Enge, Global Positioning System—Signals, Measurements and Performance, Ganga-Jamuna, Lincoln, Mass., 2001.

Pi, X., A. J. Manucci, U. J. Lindqwister, and C. M. Ho, Monitoring of global ionospheric irregularities using the worldwide GPS network, *Geophys. Res. Lett.*, *24*(18), 2283–2286, 1997.

Ratcliffe, J. A., and K. Weekes, The ionosphere, in *Physics of the Upper Atmosphere*, edited by J. A. Ratcliffe, pp. 378–470, Academic, San Diego, Calif., 1960.

Ruffini, G., A. Cardellach, L. Flores, L. Cucurull, and A. Ruis, Ionospheric calibration of Radar altimeters using GPS tomography, *Geophys. Res. Lett.*, *25*(20), 3771–3774, 1998.

Sardon, E., and N. Zarraoa, Estimation of total electron-content using GPS data—How stable are the differential satellite and receiver instrumental biases, *Radio Sci.*, *32*, 1899–1910, 1997.

Schaer, S., Mapping and predicting the Earth's ionosphere using the Global Positioning System, Ph.D. thesis of Bern Univ., 1999.

Schaer, S., G. Beutler, M. Rothacher, and T. Soringer, Daily global ionosphere maps based on GPS carrier phase data routinely produced by the CODE Analysis Center, in *Proc. IGS Analysis Center Workshop*, Silver Spring, Maryland, March 19–21, 1996.

Schaer, S., W. Gurtner, and J. Feltens, IONEX: The IONosphere Map EXchange format Version 1, in *Proceedings of the IGS Analysis Center Workshop*, edited by J. M. Dow, J. Kouba, and T. Springer, pp. 233–247, Darmstadt, February 9–11, 1998.

Van Dierendonck, A. J., J. Klobuchar, and Q. Hua, Ionospheric scintillation monitoring using commercial single frequency C/A code receivers, *Proc. Sixth International Technical Meeting of Satellite Division of the Institute of Navigation ION-GPS 93*, pp. 1333–1342, 1993.

Van Zandt, T. E., The neutral atmosphere and the quiet ionosphere, in *Physics of Geomagnetic Phenomena*, edited by S. Matsushita and W. H. Campbell, pp. 509–559, Academic, San Diego, Calif., 1967.

Wild, U., G. Beutler, W. Gurtner, and M. Rothacher, Estimating the ionosphere using one or more dual frequency GPS receivers, in *Proc. Fifth International Geodetic Symposium on Satellite Positioning*, pp. 724–736, Las Cruces, New Mexico, 13–17 March, 1989.

Wilson, B. D., and A. J. Manucci, Extracting ionospheric measurements from GPS in the presence of Anti-Spoofin, in *Proc. Seventh International Technical Meeting of the Satellite Division of the Institute of Navigation ION-GPS 94*, 1599–1608, 1994.

Wilson, B. D., A. J. Manucci, and C. D. Edwards, Subdayly Northern Hemisphere maps using an extensive network of GPS receivers, *Radio Sci.*, *30*(3), 639–648, 1995.

C. Brunini, Facultad de Ciencias Astronomicas y Geofísicas, Universidad Nacional de La Plata, Paseo del Bosque s/n, 1900 La Plata, Argentina. (claudio@fcaglp.unlp.edu.ar)

M. Gende and A. Meza, Universidad Nacional de La Plata and CONICET, Georefereciacion Satelital, Facultad de Ciencias Astronomicas y Geofisicas, La Plata 1900, Argentina. (mgende@fcaglp.unlp.edu.ar)

M. A. Van Zele, Facultad de Ciencias Exactas y Naturales–Departamento de Ciencias Geológicas-Geofisica, Ciudad Universitaria, C1428EHA Buenos Aires, Argentina. (aváncele@gl.fcen.uba.ar)